



# A circular polarization converter based on in-linked loop antenna frequency selective surface

Shen-Yun Wang<sup>1</sup> · Wei Liu<sup>1</sup> · Wen Geyi<sup>1</sup>

Received: 8 January 2018 / Accepted: 1 June 2018 / Published online: 4 June 2018  
© Springer-Verlag GmbH Germany, part of Springer Nature 2018

## Abstract

In this paper, we report the design, fabrication and measurement of a circular polarization converter based on an in-linked loop-antenna frequency selective surface. The building unit cell is the in-linked loop-antenna module, which consists of same front and back planar loop antennas in-linked by a pair of through-via holes passing through a sandwiched perforated metal ground plane. The proposed device can achieve transmission polarization conversions from right- or left-handed circularly polarized waves to left- or right-handed ones, respectively, or vice versa. Simulation and experimental results show that it has relative conversion ratio of near unity at resonant frequency and very low Joule insertion loss in the operating frequency band. The proposed circular polarization converter may be applied to wireless systems where circular polarization diversity is needed.

## 1 Introduction

Circular polarization converters are polarization control devices which can convert incident waves with given polarization states to reflected or transmitted right- or left-handed circularly polarized (RHCP or LHCP) ones. They are key elements in satellite communication systems and remote sensing devices as circularly polarized (CP) waves can reduce the signal loss efficiently and eliminate the polarization influence caused by Faraday rotation effect in ionosphere [1–3]. Although CP waves can be created by antenna itself, an alternative and effective way is to generate a linearly polarized (LP) wave and pass it through a transmission-type circular polarization converter [4–7]. The latter is important and of flexibility, and for instance it can be applied to switch a satellite's antenna from one polarization to circular polarization with a demanded handedness.

Conventional converters in optical, infrared and terahertz regimes are typically realized using birefringence or chiral effect of anisotropic materials, such as wave plates [8, 9]. However, due to the lack of natural anisotropic materials in microwave and millimeter waves, the circular polarization

converters are generally implemented using frequency selective surfaces (FSSs) [7, 10–22], metasurfaces [23–30] and some other artificially periodic metamaterials [31–34]. Compared with structure of metasurfaces and metamaterials for electromagnetic (EM) wave polarization conversions, whose unit cell dimensions are usually in sub-wavelength scale [23–39], the building element of FSSs has the merit of larger dimensions, which can thus reduce the fabrication precision requirement, and associated complexity and costs.

For the reasons mentioned above, different structures for building the elements of FSSs have been proposed to realize circular polarization converters, such as the meander lines [10–13], patch and wire grid configurations [14, 15], slot resonators [16, 17], split-ring resonators [18, 19], and antenna-filter-antenna (AFA) modules [22]. Most circular polarization converters convert LP waves into RHCP or LHCP ones. The building elements of the FSSs are usually orthotropic structures, and the incident LP wave can be divided into two equal orthogonal components. If there is a differential phase shift of nearly  $90^\circ$  between the two field components in the transmission, but with identical amplitudes, the incident LP wave will be converted to a CP one. A circular polarization converter can also achieve the conversions from RHCP waves to LHCP ones [32], which have important applications in microwave imaging systems. For example, it has been proved in human body security check imaging system that smooth human body image or highlighted concealed weapon image can be obtained by using

✉ Shen-Yun Wang  
wangsy2006@126.com

<sup>1</sup> Research Center of Applied Electromagnetics, Nanjing University of Information Science and Technology, Nanjing 210044, China

antennas with different circular co- and cross-polarization combinations [10]. However, the circular polarization converter presented in Ma et al. [32] can only convert RHCP waves to LHCP ones due to the asymmetrical configuration of the bi-layered split-ring resonators. The conversion principle is explained by the extrinsic chirality in the forward propagation direction, and the polarization conversion efficiency is not very high due to the near-field coupling between the front and back split-ring resonators.

In this paper, we propose an alternative approach to the design of circular polarization converters using an in-linked loop-antenna module-based FSS structure. The building module consists of a planar loop-antenna pair and is internally connected by a pair of through-via holes. The front planar loop-antenna resonator array functions as a RHCP or LHCP wave receiver, and the backside one transmits CP wave with different handedness in the forward propagation direction, and the through-via pair play a role of high efficiency transverse electric and magnetic (TEM) wave coupler with extremely low radiating loss. Due to the TEM wave coupling using the through-via pair, instead of near-field coupling used in previous studies, very high conversion efficiency and low insertion loss can be achieved.

## 2 Design schemes

Antenna-filter-antenna (AFA) module-based FSS was first proposed in literature [40], which has the advantages of high frequency selectivity and simple configuration. The design approach of AFA FSS is simpler compared with that of the conventional multilayer FSSs. Each AFA module is composed of a receiving antenna, a non-radiating resonant structure, and a transmitting antenna [40]. The aperture coupled-patch structure was the most typical AFA module as investigated in literatures [40, 41]. Using one kind of AFA module, a linear to circular polarization converter is presented [22], wherein a circular aperture is introduced within the common ground as the non-radiating resonant structure, such that the two patches were coupled through the circular aperture to achieve a second-order band-pass response.

Motivated by this designing approach, we present an in-linked loop-antenna structure as a new kind of AFA module as the FSS building block to realize the transmission circular polarization conversion from RHCP waves to LHCP ones in microwave C-band. The proposed in-linked loop-antenna module consists of a planar loop-antenna pair and internally connected by a pair of through-via holes acting as a quasi-two-wire transmission line, as shown in Fig. 1.

The scheme of a sample array is illustrated in Fig. 1a, where the in-linked loop-antenna module is optimized to operate at frequency of 5.9 GHz, and the dimensions are found to be:  $L = 12.0$  mm,  $R_1 = 2.5$  mm,  $R_2 = 5.65$  mm,

$g = 0.3$  mm,  $h = 3.035$  mm and  $t = 0.035$  mm, where  $h$  and  $t$  represent the thickness of substrate layer and metal film, respectively, as shown in Fig. 1b. For clarity, the unit cell illustrated in Fig. 1b is decomposed into three metal layers as shown in Fig. 1c–e, respectively. The front loop-antenna resonator is connected with the back one by a through-via pair, which passes through the sandwiched perforated common ground plane. Both the front and backside loop-resonators are fabricated on a dielectric substrate. The double-layer substrates are chosen to be Rogers RO4003 with a dielectric constant of 3.55 and loss tangent of 0.0027. The optimization and simulation are carried out using commercial software, Ansoft High Frequency Structure Simulator (HFSS), and the frequency domain solver was chosen with periodic boundary condition in both transverse directions and the Floquet ports in the wave propagating direction to extract scattering parameters.

Here, we define the reflection and transmission coefficients as  $R_{ij}$  and  $T_{ij}$ , respectively, where the indices  $i$  and  $j$  correspond to the polarization states of the incident and transmitted EM waves, which could be RHCP wave ( $i$  or  $j$  is represented by +) and LHCP wave ( $i$  or  $j$  is represented by –). Figure 2a shows the magnitude of the reflection and transmission coefficients when a RHCP wave is normally impinging onto the presented circular polarization converter. From the figure, we find that the presented polarization converter has a band-pass response in circularly cross-polarized transmission ( $T_{-+}$ ) mode (transmitted LHCP mode) with its central resonant frequency of 5.9 GHz (nearly  $-0.21$  dB), while the amplitude of circularly co-polarized transmission ( $T_{++}$ ) mode (transmitted RHCP mode) and co- and cross-polarized reflection ( $R_{++}$  and  $R_{-+}$ ) modes (reflected RHCP and LHCP modes) are all less than  $-22$  dB, indicating they are very close to zero. Due to the structural symmetry of the designed loop-antenna resonator, the circular polarization converter is independent of the handedness of incident CP wave and propagation direction. It means that incident LHCP waves can also be converted into RHCP ones in transmission mode, and the reversed conversions in the backward propagating direction also can be achieved. To understand the polarization conversion, the incident and transmitted CP waves can be decomposed into two orthogonal linear components. For the forward RHCP wave incidence, the amplitudes and phase shifts of decomposed linear components of the transmitted wave are shown in Fig. 2b, c, respectively. At resonant frequency 5.9 GHz, the amplitudes of the orthogonal linear components are both near  $-3.0$  dB, and the phase shift of the vertical component is  $90^\circ$  ahead of the horizontal one, indicating that a transmitted LHCP wave with both the axial ratio (AR) and conversion efficiency being of near unity is generated. In the higher frequency band ranging from 5.9 to 7.0 GHz, the decomposed amplitudes are identical and the difference of phase shifts remains  $90^\circ$ , which

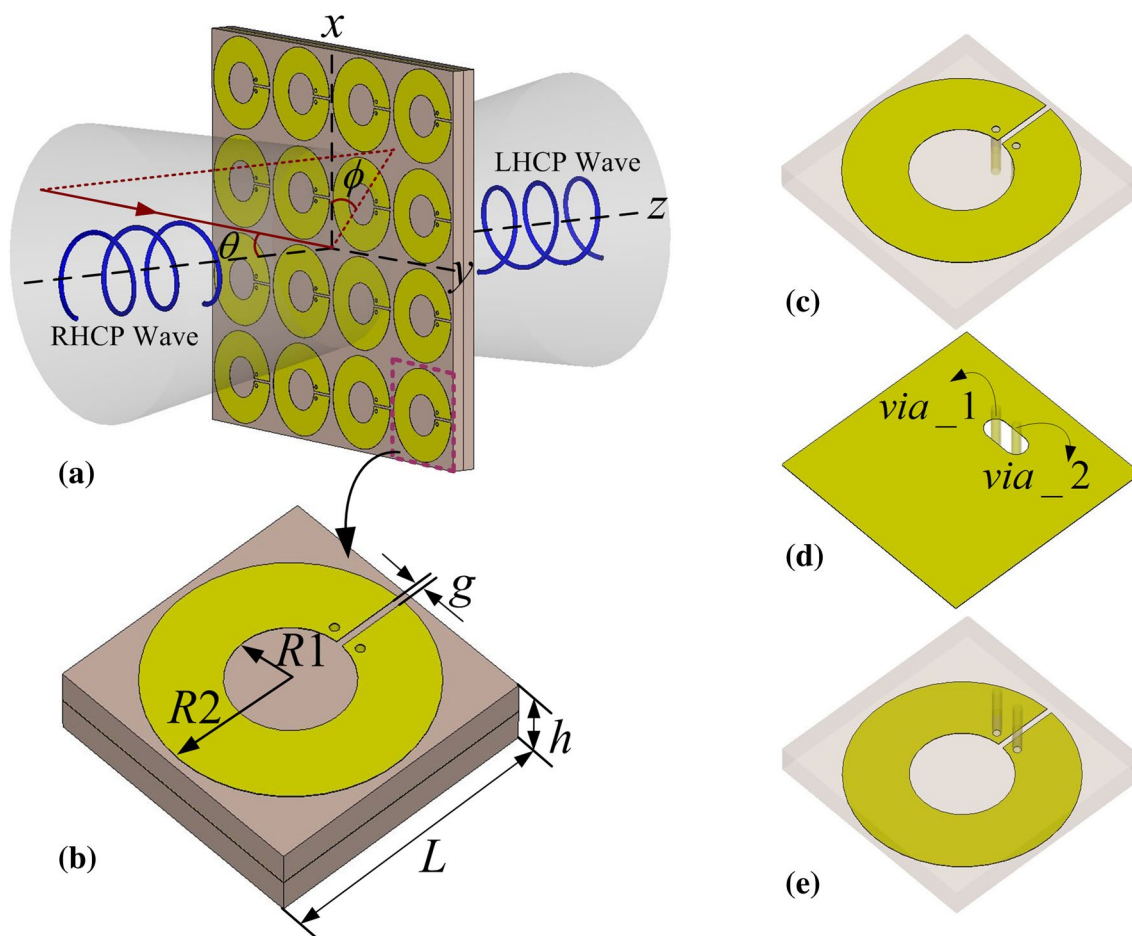


**Fig. 1** **a** Scheme of sample array, **b** the building block, **c** the front loop-antenna resonator, **d** the perforated common ground plane and **e** the backside loop-antenna resonator

implies that the transmitted LHCP wave has an axial ratio of near unity in a wide frequency band.

To better evaluate the performances of the proposed circular polarization converter, the Joule insertion loss (IL) and relative circular cross-polarization conversion efficiency (RCP) have been calculated, respectively, using the following formulas:

$$IL = 1 - |R_{++}|^2 - |R_{-+}|^2 - |T_{++}|^2 - |T_{-+}|^2, \tag{1}$$

and

$$RCP = \frac{|T_{-+}|^2}{|R_{++}|^2 + |R_{-+}|^2 + |T_{++}|^2 + |T_{-+}|^2}. \tag{2}$$

The calculated result of insertion loss is shown in Fig. 2d, and the value of IL is less than 3.0% in the operating frequency band, and the maximum IL value occurs at the resonant frequency 5.9 GHz. For there is nearly no circularly co- and cross-polarized return loss and co-polarized

transmission loss, the absolute circular cross-polarized transmittance is nearly up to 97% at the resonant frequency. If we ignore the insertion loss, the RCP curve in Fig. 2d indicates that an almost unity conversion efficiency at the resonant frequency has been obtained.

To demonstrate the working mechanism of the proposed in-linked loop-antenna module-based FSS circular polarization converter, the induced current distributions at the resonant frequency on the metal components are depicted in Fig. 3. The front planar loop-antenna responds to the incident CP wave with one handedness and the induced current on each element propagate along the through-via holes in TEM mode. The propagating current is converted into a radiated CP wave with another handedness by the backside planar loop-antenna. When a RHCP wave is normally incident onto the sample, a peak of the induced current moves around clockwise as the increase of phase, indicating the coupling with the incident RHCP wave. Figure 3a–c illustrates the current distribution on the front and backside loop-antenna resonators and the through-via pair

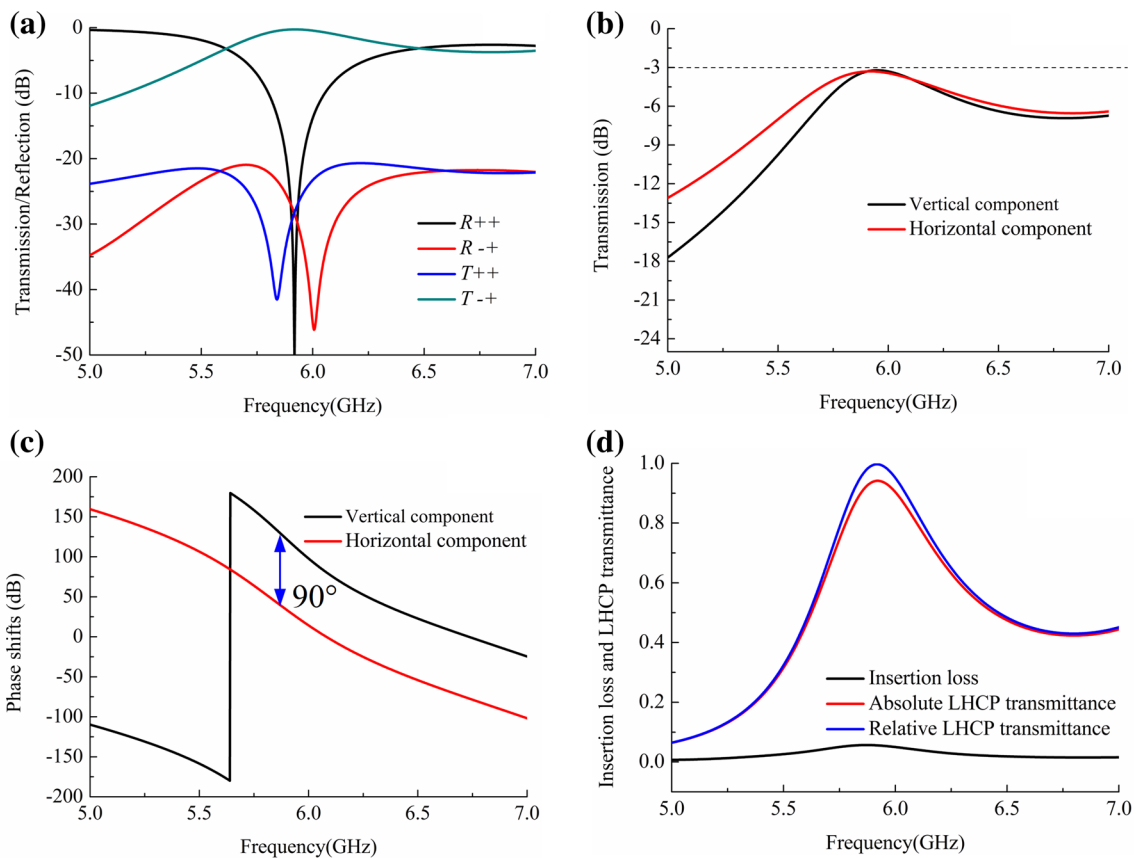


**Fig. 2** **a** Amplitudes of the transmission and reflection of the CP wave converter, **b** the transmitted amplitudes and **c** phase-shift difference of the decomposed components for the transmitted LHCP wave, **d** the insertion loss and LHCP wave transmittance

as time increases, and the snapshots relate to the phases of  $0^\circ$ ,  $30^\circ$  and  $60^\circ$ , respectively. For clarity, the configuration has been decomposed into three parts and the connecting points between the through-via holes and loop-antennas are labeled with  $A$ ,  $A'$ ,  $B$  and  $B'$ , respectively. The current peak on the backside loop-antenna resonator reverses with respect to the front one, e.g. another peak value of the current moves around counterclockwise on the backside loop-antenna, and results in outgoing LHCP wave.

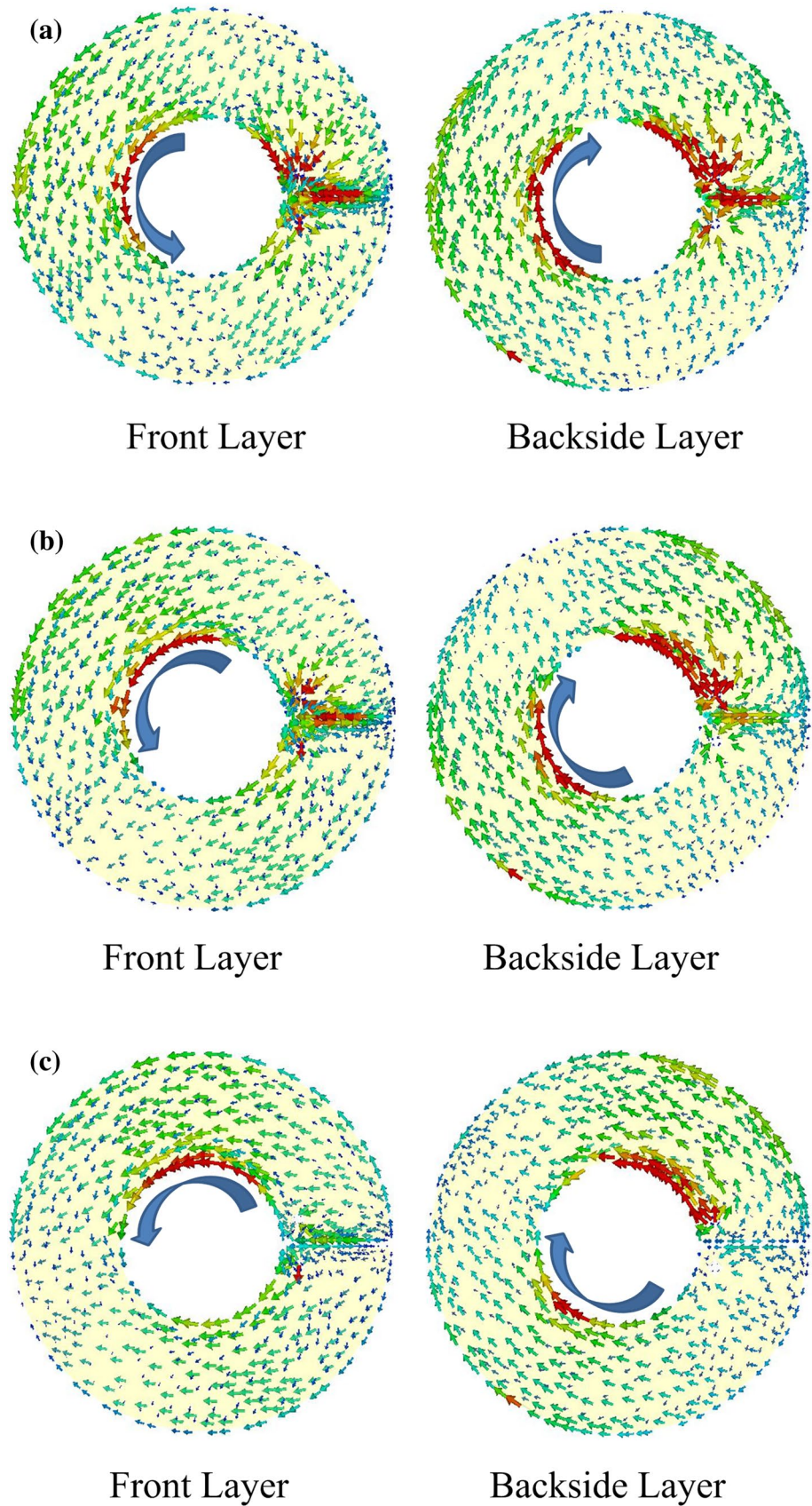
### 3 Experimental results and discussion

The designed circular polarization converter is fabricated by utilizing the conventional printed circuit board with the same structural parameters as the simulation model. The photograph of the sample is shown in Fig. 4, which has dimensions of  $300 \times 300$  mm, containing  $25 \times 25$  building elements. Measurements are performed in an anechoic chamber, and the fabricated sample is embedded in a microwave absorbing screen to avoid unwanted reflections. Figure 4 also shows the schematic of the experimental setup.

As illustrated in Fig. 1a, both the circular cross-polarized reflection and co-polarized transmission are less than  $-22$  dB in the frequency band ranging from 5.0 to 7.0 GHz, and can thus be ignored in measurement. For the measurement of cross-polarized transmission, two circular wave horn antennas with different handedness are placed in the front and back sides of the test sample, respectively. The measured transmission coefficient is also normalized with that of air background. For the setup of circular co-polarized reflection, the circular transmitting and receiving horns with same handedness are nearly parallel placed (with intersection angle less than  $10^\circ$ ) in the front of the sample. The measured reflection coefficient is normalized with respect to a metal plane of same dimensions as the testing sample. Figure 5a, b shows the magnitudes of the circularly co-polarized reflection and cross-polarized transmission coefficients, respectively. The measured results agree very well with the simulation results, and the small deviations are likely caused by tolerances in fabrication and measurement.

The analysis described above is based on the situation with normal incident CP waves. However, in practice, the incident wave may be oblique or deflected due to the antenna radiation pattern or installation inaccuracy. Therefore, the

**Fig. 3** Induced current distribution of the metal components at resonant frequency in different phases: **a**  $0^\circ$ , **b**  $30^\circ$ , **c**  $60^\circ$



robustness of the circular polarization converter under oblique incidence should be evaluated. Figure 6a shows the cross-polarized transmission coefficient results with azimuth

angle  $\phi=0^\circ$  under different incident angles. Both the resonant frequency and amplitude of circularly cross-polarized transmission remain unchanged when the incident angle  $\theta$  is

Fig. 4 Fabricated device sample and the experimental setup

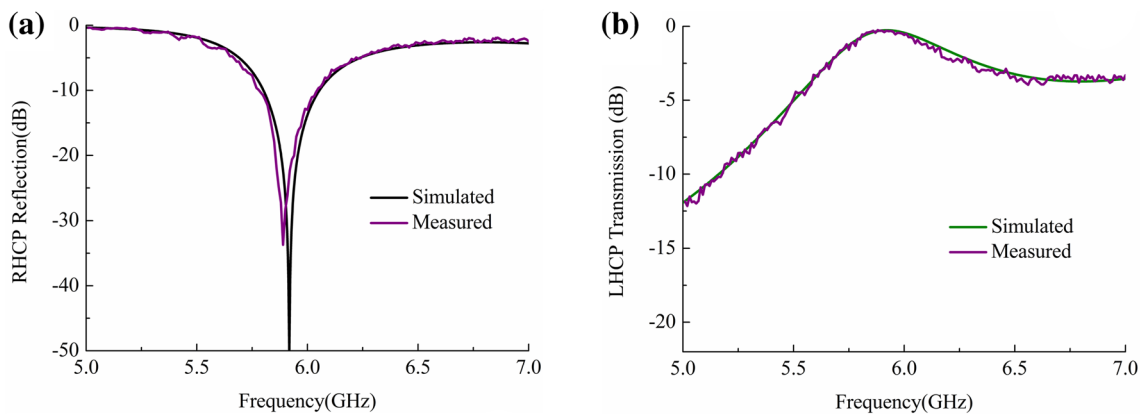
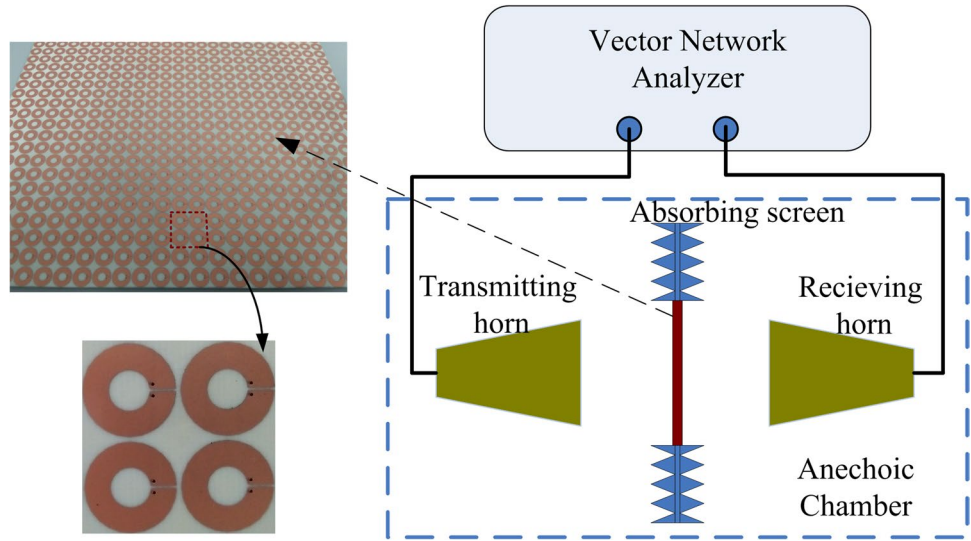


Fig. 5 Circularly a co-polarized reflection, and b cross-polarized transmission obtained by experimental measurement and numerical simulation

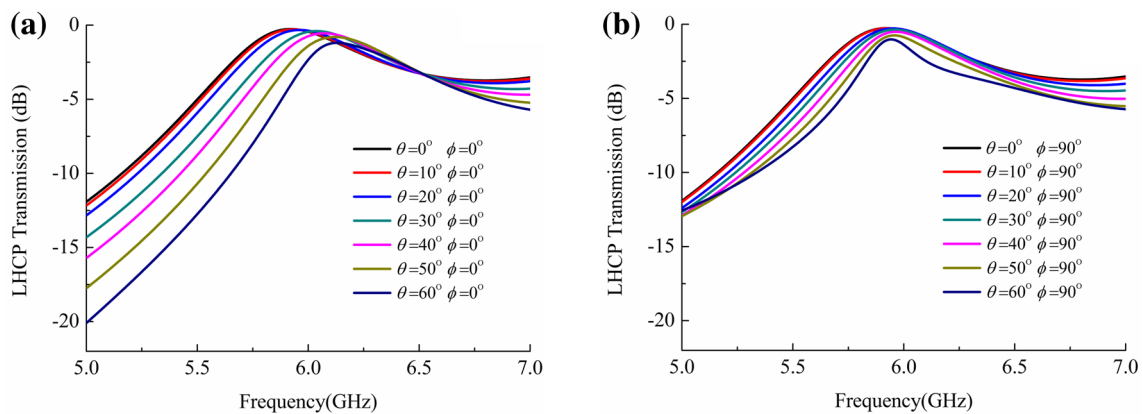


Fig. 6 Circularly cross-polarized transmission under different incident angles with azimuth angle of a  $\phi=0^\circ$  and b  $\phi=90^\circ$

less than  $20^\circ$ . Figure 6b shows the circularly cross-polarized transmission coefficient results with azimuth angle  $\phi = 90^\circ$  under different incident angles. The polarization conversion efficiency and resonant frequency are approximately independent of the incident angle when it is less than  $30^\circ$ . As the incident angle increases further, the amplitude of polarization conversion efficiency starts to decrease, while the resonant frequency remains unchanged. The above simulation results indicate that the proposed circular polarization converter is robust with the variation of incident angles in the two orthotropic azimuth angles ( $\phi = 0^\circ$  and  $90^\circ$ ).

## 4 Conclusions

In conclusion, a circular polarization converter based on an in-linked loop-antenna frequency selective surface has been proposed, fabricated and characterized, which can achieve relative circular cross-polarization conversion efficiency of near unity for incident CP waves with either right or left handedness at the desired resonant frequency under a wide range of incident angles. It should be mentioned that the design idea can be extended to other electromagnetic wave frequency bands.

**Acknowledgements** The authors acknowledge the financial support of National Natural Science Foundation of China (Grant no. 61302048), the Natural Science Foundation of Jiangsu Province of China (Grant no. BK20151528), and a project funded by the Priority Academic Program Development of Jiangsu Higher Education Institutions.

## References

- H.A. Zebker, J.J. Van Zyl, Imaging radar polarimetry: a review. *Proc. IEEE* **103**(11), 1057–1070 (1991)
- C. Dietlein, A. Luukanen, Z. Popović, E. Grossman, A w-band polarization converter and isolator. *IEEE Trans. Antennas Propag.* **55**(6), 1804–1809 (2007)
- E. Dumanis, G. Goussetis, J.L. Gómez-Tornero, R. Cahill, V. Fusco, Anisotropic impedance surfaces for linear to circular polarization conversion. *IEEE Trans. Antennas Propag.* **60**(1), 212–219 (2012)
- E. Arnaud, R. Chantalat, M. Koubeissi, T. Monediere, E. Rodes, M. Thevenot, Global design of an EBG antenna and meander-line polarizer for circular polarization. *IEEE Antennas Wirel. Propag. Lett.* **9**, 215–218 (2010)
- X. Ma, C. Huang, W. Pan, B. Zhao, J. Cui, X. Luo, A dual circularly polarized horn antenna in Ku-band based on chiral metamaterial. *IEEE Trans. Antennas Propag.* **62**(4), 2307–2311 (2014)
- X. Ma, C. Huang, M. Pu, C. Hu, Q. Feng, X. Luo, Single-layer circular polarizer using metamaterial and its application in antenna. *Microw. Opt. Technol. Lett.* **54**(7), 1770–1774 (2012)
- C. Zhang, Y. Wang, F. Zhu, G. Wei, J. Li, C. Wu, S. Gao, H. Liu, A planar integrated folded reflect array antenna with circular polarization. *IEEE Trans. Antennas Propag.* **65**(1), 385–390 (2017)
- J.B. Masson, G. Gallot, Terahertz achromatic quarter-wave plate. *Opt. Lett.* **31**(2), 265–267 (2006)
- C.Y. Chen, T.R. Tsai, C.L. Pan, R.P. Pan, Room temperature terahertz phase shifter based on magnetically controlled birefringence in liquid crystals. *Appl. Phys. Lett.* **83**(22), 4497 (2003)
- P. Fei, Z. Shen, X. Wen, F. Nian, A single-layer circular polarizer based on hybrid meander line and loop configuration. *IEEE Trans. Antennas Propag.* **63**(10), 4609–4614 (2015)
- I.L. Morrow, P. Thomas, Compact frequency selective surface for polarization transform. *Electron. Lett.* **50**(2), 64–65 (2014)
- M.A. Joyal, J.J. Laurin, Analysis and design of thin circular polarizers based on meander lines. *IEEE Trans. Antennas Propag.* **60**(6), 3007–3011 (2012)
- M.A. Joyal, J.J. Laurin, Design and analysis of a cascade circular polarization selective surface at K band. *IEEE Trans. Antennas Propag.* **62**(6), 3043–3053 (2014)
- L. Li, Y. Li, Z. Wu, F. Huo, Y. Zhang, C. Zhao, Novel polarization-reconfigurable converter based on multilayer frequency-selective surfaces. *Proc. IEEE* **103**(7), 1057–1070, (2015)
- S.M.A.M.H. Abadi, N. Behdad, Wideband linear-to-circular polarization converters based on miniaturized-element frequency selective surfaces. *IEEE Trans. Antennas Propag.* **64**(2), 525–534 (2016)
- M. Euler, V. Fusco, R. Dickie, R. Cahill, J. Verheggen, Sub-mm wet etched linear to circular polarization FSS based polarization converters. *IEEE Trans. Antennas Propag.* **59**(8), 3103–3106 (2011)
- M. Euler, V. Fusco, R. Cahill, R. Dickie, 325 GHz single layer sub-millimeter wave FSS based split slot ring linear to circular polarization convertor. *IEEE Trans. Antennas Propag.* **58**(7), 2457–2459 (2010)
- S. Yan, G.A.E. Vandenbosch, Compact circular polarizer based on chiral twisted double split-ring resonator. *Appl. Phys. Lett.* **102**(10), 103503 (2013)
- L. Martinez-Lopez, J. Rodriguez-Cuevas, J.I. Martinez-Lopez, A.E. Martynyuk, A multilayer circular polarizer based on bisected split-ring frequency selective surfaces. *IEEE Antennas Wirel. Propag. Lett.* **13**, 153–156 (2014)
- J.Q. Hou, L.F. Shi, S. Chen, Z.R. Gou, Compact broadband circular polariser based on two-layer frequency-selective surfaces. *Electron. Lett.* **51**(15), 1134–1136 (2015)
- J.Y. Yin, X. Wan, J. Ren, T.J. Cui, A circular polarizer with beam-forming feature based on frequency selective surfaces. *Sci. Rep.* **7**, 41505 (2017)
- B. Lin, J.L. Wu, X.Y. Da, W. Li, J.J. Ma, A linear-to-circular polarization converter based on a second-order band-pass frequency selective surface. *Appl. Phys. A* **123**(1), 43 (2017)
- L. Zhang, P. Zhou, H. Lu, H. Chen, J. Xie, L. Deng, Ultra-thin reflective metamaterial polarization rotator based on multiple plasmon resonances. *IEEE Antennas Wirel. Propag. Lett.* **14**, 1157–1160 (2015)
- Y. Liu, S. Xia, H. Shi, A. Zhang, Z. Xu, Dual-band and high-efficiency polarization converter based on metasurfaces at microwave frequencies. *Appl. Phys. B* **122**(6), 178 (2016)
- L. Zhang, P. Zhou, H. Chen, H. Lu, J. Xie, L. Deng, Broadband and wide-angle reflective polarization converter based on metasurface at microwave frequencies. *Appl. Phys. B* **120**(4), 617–622 (2015)
- H.L. Zhu, S.W. Cheung, K.L. Chung, T.I. Yuk, Linear-to-circular polarization conversion using metasurface. *IEEE Antennas Wirel. Propag. Lett.* **61**(9), 4615–4623 (2013)
- H. Chen, H. Ma, J. Wang, S. Qu, Y. Pang, M. Yan, Y. Li, Ultra-wideband transparent  $90^\circ$  polarization conversion metasurfaces. *Appl. Phys. A* **122**(4), 463 (2016)
- G. Zhou, X. Tao, Z. Shen, G. Zhu, B. Jin, L. Kang, W. Xu, J. Chen, P. Wu, Designing perfect linear polarization converters using perfect electric and magnetic conducting surfaces. *Sci. Rep.* **6**, 38925 (2016)

29. Z. Li, W. Liu, H. Cheng, S. Chen, J. Tian, Realizing broadband and invertible linear-to-circular polarization converter with ultrathin single-layer metasurface. *Sci. Rep.* **5**, 18106 (2015)
30. W. Wang, Z. Guo, R. Li, J. Zhang, A. Zhang, Y. Li, Y. Liu, X. Wang, S. Qu, L-shaped metasurface for both the linear and circular polarization conversions. *J. Opt.* **17**(6), 065103 (2015)
31. F. Li, L. Zhang, P. Zhou, H. Zhou, H. Chen, R. Zhao, Y. Zhou, D. Liang, H. Lu, L. Deng, Dual-band reflective polarization converter based on slotted wire resonators. *Appl. Phys. B* **124**(2), 28 (2018)
32. X. Ma, W. Pan, C. Huang, M. Pu, Y. Wang, B. Zhao, J. Cui, C. Wang, X. Luo, An active metamaterial for polarization manipulating. *Adv. Opt. Mater.* **2**(10), 945–949 (2015)
33. Y. Tamayama, K. Yasui, T. Nakanishi, M. Kitano, A linear-to-circular polarization converter with half transmission and half reflection using a single-layered metamaterial. *Appl. Phys. Lett.* **105**(2), 021110 (2014)
34. L. Wu, Z. Yang, Y. Cheng, R. Gong, M. Zhao, Y. Zheng, J. Duan, X. Yuan, Circular polarization converters based on bi-layered asymmetrical split ring metamaterials. *Appl. Phys. A* **116**(2), 643–648 (2014)
35. H. Li, B. Xiao, X. Huang, H. Yang, Multiple-band reflective polarization converter based on deformed f-shaped metamaterial. *Phys. Scr.* **90**(3), 035806 (2015)
36. K. Chen, Y. Feng, L. Cui, J. Zhao, T. Jiang, B. Zhu, Dynamic control of asymmetric electromagnetic wave transmission by active chiral metamaterial. *Sci. Rep.* **7**, 42802 (2017)
37. L. Zhang, Z. Song, H. Liu, Optical cross-polarization converter with an octave bandwidth based on anisotropic plasmonic metasurfaces. *EPL* **111**(2), 27001 (2015)
38. D.L. Markovich, A. Andryieuski, M. Zalkovskij, R. Malureanu, A.V. Lavrinenko, Metamaterial polarization converter analysis: limits of performance. *Appl. Phys. B* **112**(2), 143–152 (2013)
39. M. Fartookzadeh, Multi-band metamirrors for linear to circular polarization conversion with wideband and wide-angle performances. *Appl. Phys. B* **123**(4), 115 (2017)
40. R. Pous, D.M. Pozar, Frequency-selective surface using aperture-coupled microstrip patches. *Electron. Lett.* **25**(17), 1136–1138 (1989)
41. A. Abbaspour-Tamijani, K. Sarabandi, G.M. Rebeiz, Antenna-filter-antenna arrays as a class of bandpass frequency-selective surfaces. *IEEE Trans. Microw. Theory Tech.* **52**(8), 1781–1789 (2004)